Journal of Hazardous Materials 211–212 (2012) 349–356

Contents lists available at SciVerse ScienceDirect

Journal of Hazardous Materials

journal homepage: www.elsevier.com/locate/jhazmat

# Enhanced dechlorination of trichloroethylene using electrospun polymer nanofibrous mats immobilized with iron/palladium bimetallic nanoparticles

Hui Ma[a,b], Yunpeng Huang[b], Mingwu Shen[b], Rui Guo[b], Xueyan Cao[b], Xiangyang Shi[a,b,c,*]

[a] State Key Laboratory for Modification of Chemical Fibers and Polymer Materials, Donghua University, Shanghai 201620, PR China
[b] College of Chemistry, Chemical Engineering and Biotechnology, Donghua University, Shanghai 201620, PR China
[c] CQM – Centro de Química da Madeira, Universidade da Madeira, Campus da Penteada, 9000-390 Funchal, Portugal

ARTICLE INFO

*Article history:*
Received 15 April 2011
Received in revised form 7 November 2011
Accepted 8 November 2011
Available online 17 November 2011

*Keywords:*
Fe/Pd nanoparticles
Electrospinning
Polymer nanofibers
Trichloroethylene
Dechlorination

ABSTRACT

Fe/Pd bimetallic nanoparticles (NPs) have held great promise for treating trichloroethylene (TCE)-contaminated groundwater, without the accumulation of chlorinated intermediates. However, the conventionally used colloidal Fe/Pd NPs usually aggregate rapidly, resulting in a reduced reactivity. To reduce the particle aggregation, we employed electrospun polyacrylic acid (PAA)/polyvinyl alcohol (PVA) polymer nanofibers as a nanoreactor to immobilize Fe/Pd bimetallic NPs. In the study, the water-stable PAA/PVA nanofibrous mats were complexed with Fe (III) ions via the binding with the free carboxyl groups of PAA for subsequent formation and immobilization of zero-valent iron (ZVI) NPs. Fe/Pd bimetallic NPs were then formed by the partial reduction of Pd(II) ions with ZVI NPs. The formed electrospun nanofibrous mats containing Fe/Pd bimetallic NPs with a diameter of 2.8 nm were characterized by scanning electron microscopy, energy-dispersive spectroscopy, transmission electron microscopy, thermogravimetric analysis, and inductively coupled plasma-atomic emission spectroscopy. The Fe/Pd NP-containing electrospun PAA/PVA nanofibrous mats exhibited higher reactivity than that of the ZVI NP-containing mats or colloidal Fe/Pd NPs in the dechlorination of trichloroethylene (TCE), which was used as a model contaminant. With the high surface area to volume ratio, high porosity, and great reusability of the fibrous mats immobilized with the bimetallic NPs, the composite nanofibrous mats should be amenable for applications in remediation of various environmental contaminants.



## 1. Introduction

Trichloroethylene (TCE) is one of the most common and persistent groundwater contaminants encountered at hazardous waste sites around the world, and is suspected to be carcinogenic when given in high, chronic doses to certain strains of mice and rats [1,2]. The common occurrence of TCE in the groundwater is largely due to the extensive industrial usage and its resistance to both biotic and abiotic degradation under natural conditions. The typical degradation products based on biotic degradation (e.g., microbial reductive degradation) such as dichloroethylene (DCE) and vinyl chloride (VC), are more toxic and persistent than their parent compound, TCE [3,4]. Since the limitations of biotic degradation, much effort has been devoted to abiotic reductive dechlorination in recent years [2,5–7].

Zero-valent iron nanoparticles (ZVI NPs) have been utilized for reductive dechlorination of TCE due to its environmentally benign nature, high efficiency, and low cost [8–11]. However, the ZVI NPs are metastable, and may be apt to oxidation in the open air, thereby reducing the reactivity over time. Additionally, a small portion of the intermediate dechlorination by-products that are adsorbed onto the surface of the ZVI NPs such as DCE and VC cannot be completely remediated, thereby limiting the use of ZVI NPs in field remediation [1,12]. To further improve the performance of the reductive dechlorination, bimetallic (Fe/Pd or Fe/Ni) NPs formed by plating a trace amount of a metal catalyst onto the ZVI NPs have been developed [13–15]. In particular, Fe/Pd NPs with Pd depositing onto the ZVI NP surfaces as a catalyst are able to degrade TCE more rapidly and generate saturated hydrocarbon products. The higher reactivity of the Fe/Pd bimetallic NP system is ascribed to the generation of $H_2$ from ZVI NP corrosion that can be further utilized by Pd catalyst to accelerate the reactivity [16,17]. In addition, metal Pd deposited onto the surface of ZVI NPs is able to effectively reduce the production of toxic intermediates accumulated on the surface of ZVI NPs [11,18–20].

Despite the increasing evidence demonstrating the role of Fe/Pd NPs in groundwater remediation and the process in understanding

* Corresponding author at: College of Chemistry, Chemical Engineering and Biotechnology, Donghua University, 2999 North Renmin Road, Shanghai 201620, China. Tel.: +86 21 67792656; fax: +86 21 67792306 804.
*E-mail address:* xshi@dhu.edu.cn (X. Shi).

0304-3894/$ – see front matter © 2011 Elsevier B.V. All rights reserved.
doi:10.1016/j.jhazmat.2011.11.038

the reaction mechanism of TCE degradation [7,21,22], the major concern related to the Fe/Pd NPs in the TCE remediation is that the particles tend to agglomerate primarily through direct interparticle interactions such as van der Waals forces and magnetic interactions [23]. The agglomeration of the particles results in reduced specific surface area and interfacial free energy of the particles, thereby diminishing their reactivity and transportation in practical remediation applications. To solve this problem, extensive studies have been devoted to stabilizing the NPs with various supports or stabilizers. In most circumstances, Fe/Pd NPs have been stabilized by anionic polyelectrolytes or other macromolecules to reduce aggregation and to improve transportation in groundwater. For example, Fe/Pd NPs have been stabilized using carboxymethyl cellulose (CMC) [21,23], polyacrylic acid (PAA) [11,24], and starch [13]. However, these stabilized Fe/Pd NPs are difficult to be recycled once they are dispersed in the waste water, and may generate secondary contamination. For environmental applications, it is very important to immobilize Fe/Pd NPs onto a vehicle that can be easily separated from the contaminated water. Immobilization of Fe/Pd NPs onto solid supports, such as reactive activated carbon (RAC) [20,25,26], microfiltration membrane [12,27–29] have been proven to improve the reactivity, mobility, and recyclability of the NPs to a certain extent. However, development of various approaches to immobilizing the metallic NPs to improve the environmental remediation performance still remains a great challenge.

In our previous studies, we have immobilized ZVI NPs onto or within polymer nanofibers for environmental applications [30–33]. In our approach, crosslinked water-stable electrospun PAA/polyvinyl alcohol (PVA) nanofibers were used as a nanoreactor to complex iron (III) ions with the free PAA carboxyl residues for subsequent reductive formation of ZVI NPs. The formed ZVI NP-containing polymer nanofibers are stable and are capable to decolorize dyeing water and to remove copper (II). With the high surface area to volume ratio, high porosity, and great reusability, the developed ZVI NP-containing polymer nanofibrous mats display good performance in environmental remediation applications.

In this present study, we aimed to investigate the feasibility of using PAA/PVA electrospun nanofibers as a nanoreactor to prepare Fe/Pd NPs for the degradation of TCE. The ZVI NPs immobilized within PAA/PVA nanofibers were exposed to Pd (II) solution, then Fe/Pd bimetallic NPs were formed by partial reduction of $Pd^{2+}$ with ZVI NPs. The formed Fe/Pd NP-containing polymer nanofibers were characterized by scanning electron microscopy (SEM), energy-dispersive spectroscopy (EDS), transmission electron microscopy (TEM), Fourier transform infrared (FTIR) spectroscopy, thermogravimetric analysis (TGA), and inductively coupled plasma-atomic emission spectroscopy (ICP-AES). The ability and reusability to efficiently remediate TCE was also tested. To our knowledge, this is the first report related to the immobilization of bimetallic Fe/Pd NPs within polymer nanofibers for environmental remediation applications.

## 2. Experimental

### 2.1. Materials

PAA (average $M_w$ = 240,000, 25% in water) was obtained from Aldrich. PVA (88% hydrolyzed, average $M_w$ = 88 000) and sodium borohydride were from J&K Chemical (China). Iron chloride hexahydrate ($FeCl_3{\cdot}6H_2O$), palladium chloride ($PdCl_2$), and TCE solution were purchased from Sinopharm Chemicial Reagent Co., Ltd. (China). Water used in all experiments was purified using a Milli-Q Plus 185 water purification system (Millipore, Bedford, MA) with resistivity higher than 18 MΩ cm.

### 2.2. Preparation of crosslinked PAA/PVA nanofibrous mats

PAA/PVA nanofibrous mats were prepared by electrospinning a 12 wt% PAA/PVA mixture solution according to literature with a slight modification [33]. Specifically, PVA solution was prepared by dissolving PVA powder into water at 80 °C for 3 h under magnetic stirring, and then the solution was cooled down to room temperature and stored in refrigerator before use. The measured PVA and the PAA aqueous solutions were mixed with a mass ratio of 1:1 under magnetic stirring overnight to achieve a homogeneous solution. The freshly prepared polymer mixture solution was loaded into a syringe with a needle having an inner diameter of 0.8 mm. The flow rate was controlled by a syringe pump (JZB-1800, Jia Yuan Medical Technology Co., Ltd., China) at 0.5 mL/h. The high voltage power supplier (BGG40/2, Institute of Beijing High voltage Technology, China) was connected to a nozzle by a high-voltage insulating wire with two clamps at the end. The collector was covered with aluminum foil with a tip-to-collector distance of 25 cm and was grounded directly. The electrospinning setup can be found in our previous reports [32,34]. At an applied voltage of 16.6 kV, the polymer jets emerged from the Taylor Cone under the high electrical field formed ultra-fine fibers, which were collected on the aluminum foil. Freshly prepared PAA/PVA nanofibrous mats were crosslinked by thermal treatment in an oven at 145 °C for 30 min to render them water stable according to literature [33].

### 2.3. Preparation of Fe/Pd NPs immobilized within PAA/PVA nanofibrous mats

The crosslinked nanofibrous mats were dipped into an aqueous ferric trichloride solution (0.18 M) for 3 h to allow ferric ions to complex with available free PAA carboxyl groups through ionic exchange, followed by rinsing with water three times to remove non-complexed Fe(III) ions. ZVI NPs immobilized in the PAA/PVA nanofibrous mats were formed by reducing the Fe(III) ions using sodium borohydride solution (0.94 M) for 30 min. The reduction reaction was processed as the following:

$$4Fe^{3+} + 3BH_4^- + 9H_2O \rightarrow 4Fe^0\downarrow + 3H_2BO_3^- + 12H^+ + 6H_2\uparrow \quad (1)$$

The formed ZVI NP-containing nanofibrous mats were rinsed three times with water, and then immersed into an acetone solution of palladium chloride (1.8 mM) for 1 h. The Fe/Pd NPs were formed by deposition of Pd on the ZVI NP surfaces through the following reaction:

$$Pd^{2+} + Fe^0 \rightarrow Pd^0 + Fe^{2+} \quad (2)$$

The PAA/PVA nanofibrous mats containing Fe/Pd NPs were rinsed with ethanol and water three times, respectively, followed by vacuum drying at room temperature for 24 h. Finally, the Fe/Pd NP-immobilized fibrous mats were stored in a desiccator before characterization and application. Note that in all cases, the ratio of the mass of the added nanofibrous mat to the volume of the solutions of salt or reducing agents was kept at 1 mg/mL.

For control experiments, ZVI NP-containing electrospun nanofibrous mats without further deposition of Pd were prepared. Fe/Pd colloid NPs were also synthesized as a control. In brief, ferric salt solution (0.18 M, 10 mL) was directly reduced by adding a solution of sodium borohydride (0.94 M, 10 mL) under vigorous stirring for 20 min to yield colloid ZVI NPs. The ZVI NPs were centrifuged and rinsed with water, followed by soaking the ZVI NPs into an acetone solution of palladium chloride (10.8 M, 10 mL) to form Fe/Pd colloidal NPs [35]. The formed Fe/Pd colloidal NPs were centrifuged and rinsed with ethanol and water, freeze-dried, and stored in a vial before use. In addition, we also prepared Pd NP-containing PAA/PVA nanofibrous mat for another control experiment. In brief, a piece of crosslinked PAA/PVA nanofibrous mat was immersed

into a $K_2PdCl_4$ aqueous solution (4 mM) for 1 h to allow $PdCl_4^{2-}$ to complex with the nanofibers, followed by rinsing with water for three times to remove excess $PdCl_4^{2-}$. Then sodium borohydride solution (20 mM) was dropped onto the nanofibrous mat to reduce $PdCl_4^{2-}$ until no hydrogen gas to release. The formed Pd NP-containing nanofibrous mat was rinsed three times with DI water, followed by vacuum drying at room temperature for 24 h. The Pd NP-containing fibers were stored in a desiccator before use.

### 2.4. Characterization techniques

Morphologies of the electrospun nanofibrous mats were observed using SEM (TM-100, Hitachi, Japan) with an operating voltage of 10 kV. Prior to SEM measurements, samples were sputter-coated with 10 nm thick Pt films. The elemental composition of the samples was analyzed by EDS detector (IE 300X, Oxford, United Kingdom) attached to the SEM (JSM-5600LV, JEOL Ltd., Japan) at an operating voltage of 15 kV. To observe the distribution of NPs in the nanofibers, the Fe/Pd NP-immobilized polymer nanofibrous mats were embedded in epoxy resin and were cut into ultrathin sections with ultramicrotome equipped with a diamond knife. The cross-sectional images of the fibers containing Fe/Pd NPs were recorded by TEM (JEM2100, JEOL Ltd., Japan) with an operating voltage of 200 kV. The diameter of nanofibers and particles was measured using image analysis software ImageJ 1.40G (http://rsb.info.nih.gov/ij/download.html). At least 300 randomly selected nanofibers or Fe/Pd NPs in different SEM or TEM images were analyzed for each sample to acquire the diameter/size distribution histograms. TGA was carried out on a TG 209 F1 (NETZSCH Instruments Co., Ltd., Germany) thermogravimetric analyzer with a heating rate of 20 °C/min in air. FTIR spectra were recorded using a Nicolet 5700 FTIR spectrometer (Thermo Nicolet Corporation, United States) in a wavenumber range of 4000–500 $cm^{-1}$ at ambient conditions. ICP-AES (Prodigy, Leeman Laboratories Inc., America) was chosen to analyze the metal composition of the composite nanofibers.

### 2.5. Degradation of TCE

A batch experiment of TCE degradation was performed in an 800 mL beaker at room temperature. The reactor was initially filled with an aqueous TCE solution (600 mL, 10 mg/L) prepared using water that was fully deoxygenated by nitrogen gas purging. A freshly fabricated Fe/Pd NP-containing nanofibrous mat was added to the beaker under vigorous stirring to reach a final Fe concentration of 0.7 g/L. At the selected time intervals, 10 mL of the aqueous sample was withdrawn from the reactor to analyze TCE concentration using a QP-2010 gas chromatography–mass spectrometry (GC–MS) system. The TCE dechlorination efficiency was calculated according to the following equation:

$$\text{TCE dechlorination efficiency}(\%) = \frac{C_0 - C_t}{C_0} \times 100\% \quad (3)$$

where $C_0$ and $C_t$ is the initial TCE concentration and the TCE concentration at time $t$, respectively.

## 3. Result and discussion

### 3.1. Preparation and characterization of Fe/Pd NP-containing nanofibrous mats

SEM was performed to observe the morphology of the formed nanofibrous mats before and after Fe/Pd NP loading (Fig. 1). In all cases, the PAA/PVA nanofibers with or without loading of metallic NPs displayed a smooth and porous fibrous morphology with relatively uniform diameter distribution. PAA/PVA nanofibers without metal NP loading had a diameter of 217 ± 65 nm (Fig. 1a), slightly larger than that reported in our previous report [33]. This is likely due to the larger polymer concentration (12%) used for electrospinning than that used in literature (10%) since all other processing parameters remained similar. After the loading of ZVI NPs (Fig. 1b), the fiber diameter was increased to 237 ± 55 nm. Further deposition of Pd onto the ZVI NPs led to a further increase of the fiber diameter to 303 ± 52 nm (Fig. 1c). The increased fiber diameter should be caused by the swelling of nanofibers after immersing into the solution for either ZVI NP immobilization or for the follow-up deposition of Pd onto the surface of preformed ZVI NPs. For the case of Fe/Pd NP-immobilized nanofibers, the double immersion of nanofibers and further deposition of Pd resulted in the largest diameter of the final bimetallic fibers in all three cases. It is interesting to note that for the Fe/Pd NP-immobilized nanofibers, some white dots distributed along the nanofibers are likely the partially aggregated Fe/Pd NPs (Fig. 1c). In addition, the bended fiber structure after immobilization of the NPs may be ascribed to the multiple times to dip the nanofibrous mats into either aqueous or organic solutions, leading to the partially non-uniform swelling of the nanofibers.

The loading of Fe/Pd NPs within the nanofibers was confirmed by EDS analysis of the elemental composition of the nanofibers (Fig. 1d). Both Fe and Pd elements can be clearly seen in the EDS spectrum. The elemental oxygen observed could be attributed to the hydroxyl group of the PVA polymer and the carboxyl group of the PAA polymer in the nanofibers [33].

The morphology of the Fe/Pd NPs immobilized within the nanofibers was observed by cross-sectional TEM images of the bimetallic NP-containing polymer nanofibers (Fig. 2). Individual NPs with a relatively dense and uniform distribution along the cross section of nanofibers can be clearly observed in the high-resolution TEM image (Fig. 2c). The mean diameter of the Fe/Pd NPs was estimated to be 2.8 ± 0.92 nm (Fig. 2b). The formed Fe/Pd NPs are bigger than the ZVI NPs without deposition of metallic Pd as reported in literature [32,33], presumably due to the replacement reaction that stimulates the Ostwald ripening of the particles. However, these Fe/Pd NPs immobilized within the nanofibers are much smaller than those prepared using a wet chemistry approach reported in literature [12,27–29,36], suggesting that the nanofiber nanoreactor approach employed in our study is highly efficient to limit the particle growth and nucleation. It should be noted that the formed NPs are equally distributed inside and outside the fibers with a quite uniform size distribution from TEM images of the single fiber sections (Fig. 2). However, from SEM image (Fig. 1c), a very small portion of aggregated NPs was observed to distribute onto the fiber surfaces, which does not necessarily mean that the NPs formed outside the nanofibers are completely aggregated. Furthermore, high-resolution TEM image of the immobilized Fe/Pd NPs within the nanofibers can give the lattice structure of the NPs (Fig. S1, Supporting information), however, the bimetallic nature cannot be discerned. Our ICP-AES analytical data (see below) and the EDS spectrum (Fig. 1d) of the Fe/Pd NP-immobilized nanofibers clearly indicate the bimetallic nature of the immobilized NPs.

Fig. 3 depicts the FTIR spectra of PAA/PVA nanofibers (spectrum a), ZVI NP-containing nanofibers (spectrum b), and Fe/Pd NP-containing nanofibers (spectrum c). It is clear that the absorption peaks at 3350 $cm^{-1}$ and 1710 $cm^{-1}$ represent the hydroxyl group of PVA and carboxyl group of PAA, respectively. After the ZVI NPs were formed and immobilized into the electrospun nanofibers, there were some significant differences between the FTIR spectra of PAA/PVA nanofibers and ZVI NP-immobilized PAA/PVA nanofibers in the 1710–1560 $cm^{-1}$ and the 1410–1150 $cm^{-1}$ regions, which is similar to the PAA–Fe spectrum reported in the literature [37]. However, when Pd was deposited onto the ZVI NP surfaces to form Fe/Pd bimetallic NPs, the peak at 1560 $cm^{-1}$ and 1400 $cm^{-1}$

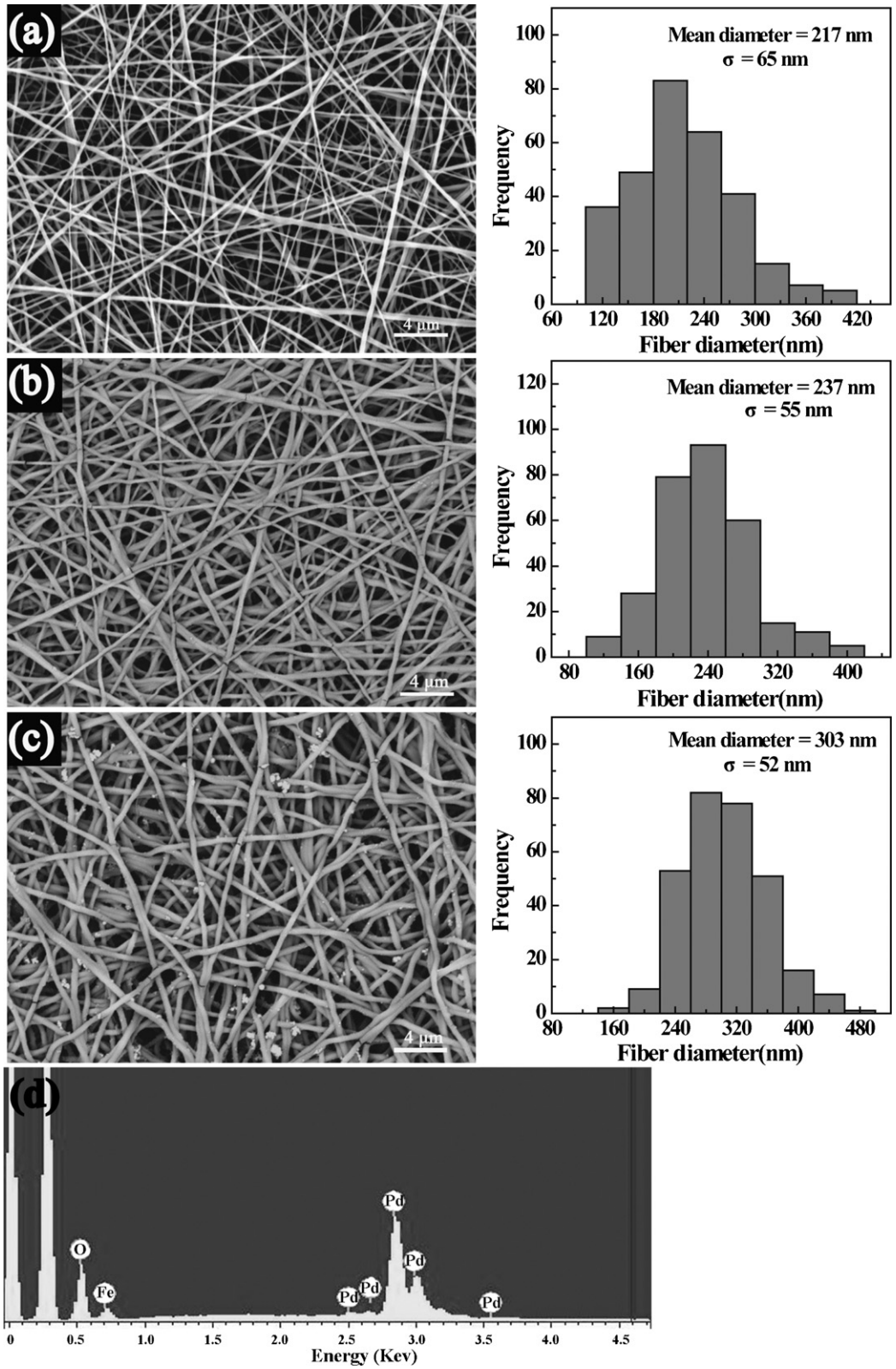


**Fig. 1.** SEM images and diameter distribution histograms of the electrospun PAA/PVA nanofibers (a), ZVI NP-containing nanofibers (b), and Fe/Pd NP-containing PAA/PVA nanofibers (c). (d) The EDS spectrum of the Fe/Pd NP-containing electrospun polymer nanofibrous mats.

disappeared and was replaced by a strong band at 1710 $cm^{-1}$ (Fig. 3, spectrum c). This is presumably due to the reaction of $Pd^{2+}$ and ZVI to form $Pd^0$ on the surface ZVI NPs. The formation of $Pd^0$ significantly shields the strong interaction of ZVI NPs and PAA carboxyl groups, setting the PAA carboxyl groups free.

TGA was used to characterize the loading capacity of ZVI NPs and Fe/Pd NPs immobilized within the cross-linked PAA/PVA nanofibrous mats (Fig. 4). The initial slight weight loss for all the nanofibers should be due to the loss of moisture in the fibers. The major weight loss of ZVI NP-containing nanofibers at the region

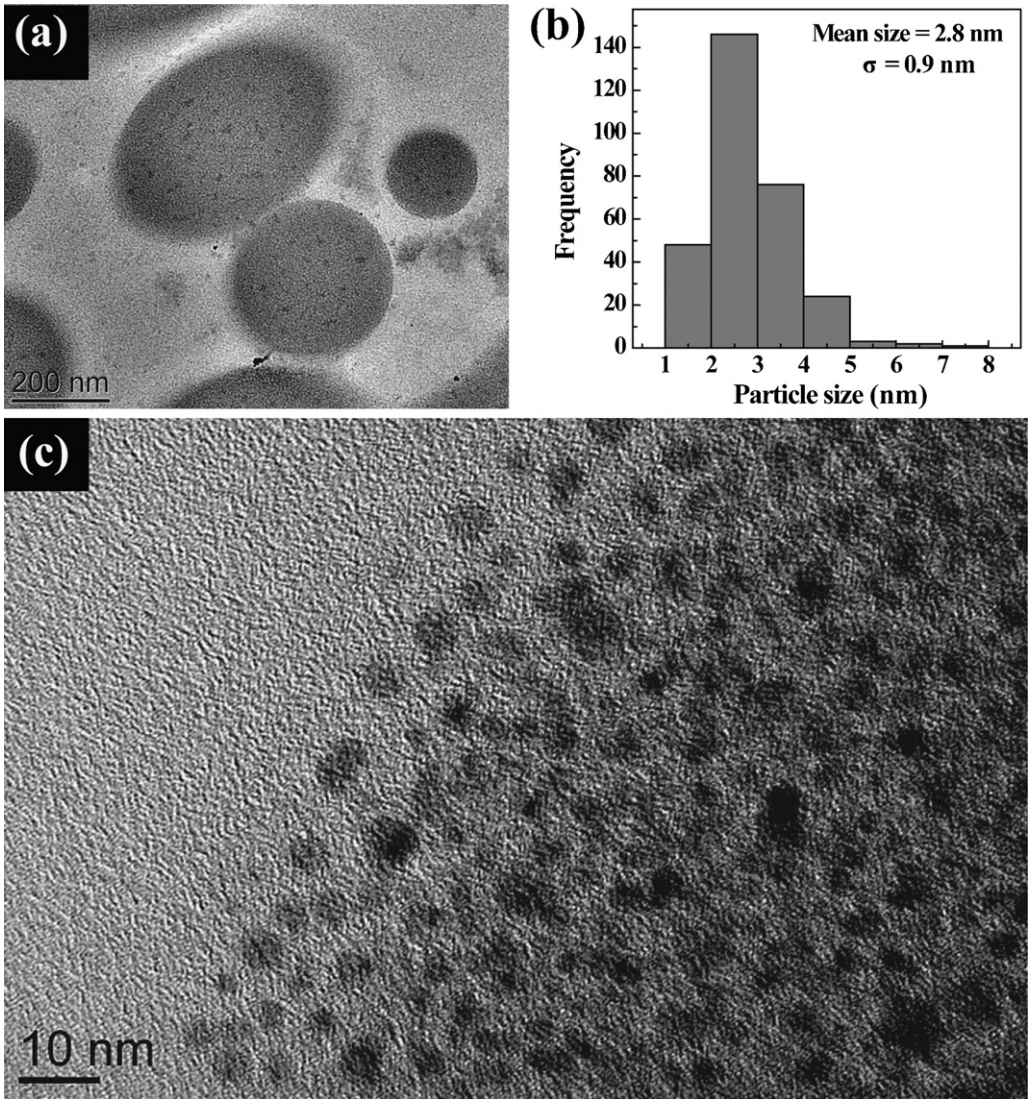


**Fig. 2.** Cross-sectional TEM (a) and high-resolution TEM (c) image of Fe/Pd NP-containing PAA/PVA nanofibers. (b) The size distribution histogram of the formed NPs.

of 170–500 °C is attributed to the decomposition of the PAA/PVA polymers. At the high temperature of 600 °C, the polymer nanofibrous mats were burned out, and iron oxide ($Fe_2O_3$) was left (Fig. 4, curve b). On the basis of this, the loading of ZVI NPs within the polymer nanofibrous mats was estimated to be approximately 20.82%, in agreement with our previous report [33]. Similarly, for Fe/Pd NP-containing nanofibers, the polymers were burned out at 600 °C and iron oxide ($Fe_2O_3$) and palladium oxide (PdO) were left

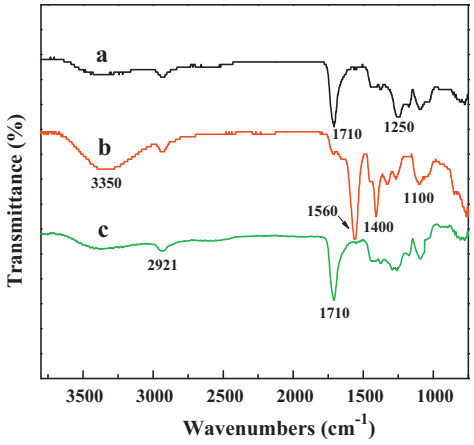


**Fig. 3.** FTIR spectra of the crosslinked electrospun PAA/PVA nanofibers (a), ZVI NP-containing PAA/PVA nanofibers (b) and Fe/Pd NP-containing nanofibers (c).

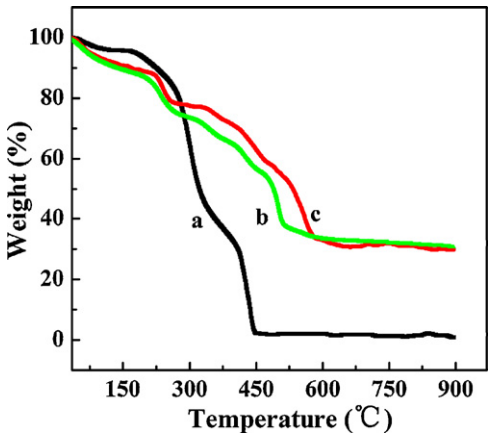


**Fig. 4.** TGA curves of the electrospun PAA/PVA nanofibrous mats without metallic NPs (a), and immobilized with ZVI NPs (b) and Fe/Pd NPs (c), respectively.

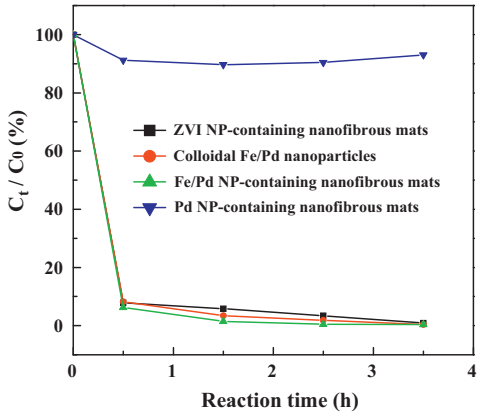


**Fig. 5.** Remaining fraction of TCE as a function of time after treatment with Fe/Pd colloid NPs, ZVI NP-containing fibrous mats, and Fe/Pd NP-containing nanofibrous mats. $C_0$ and $C$ represent the initial and final concentration of TCE, respectively. The initial concentration of TCE was 10 mg/L.

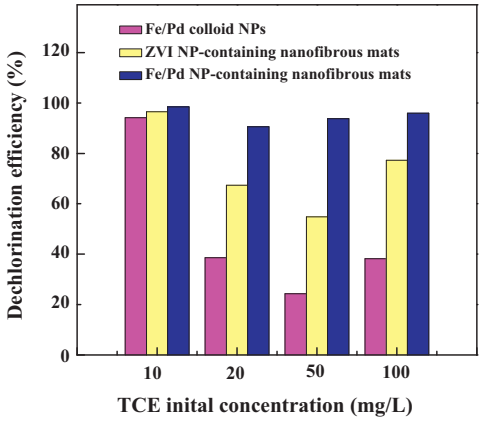


**Fig. 6.** Removal efficiency of TCE by Fe/Pd colloid NPs, ZVI NP- and Fe/Pd NP-containing nanofibrous mats with different initial TCE concentrations. The reaction time was 1.5 h.

(Fig. 4, curve c). The loading of Fe/Pd NPs within the nanofibers was estimated to be within the range of 21.49–26.71% considering the fact that the metal Pd composition is within a range of 0–100%. Further ICP-AES elemental analysis of the aqua regia extract of the bimetallic NP-immobilized nanofibers performed according to literature [35] reveals that the Fe and Pd loading is 19.44 wt% and 2.44 wt%, respectively.

### 3.2. Dechlorination of TCE using Fe/Pd NP-immobilized nanofibrous mats

TCE was selected as a model contaminant for testing the remediation capacity of the Fe/Pd bimetallic NP-loaded polymer nanofibers. Freshly synthesized Fe/Pd colloidal NPs, and ZVI NP- and Pd NP-immobilized nanofibrous mats were used as control in comparison with the performance of the bimetallic NP-containing nanofibrous mats (Fig. 5). The morphology of the formed Pd NP-immobilized nanofibrous mat was observed via SEM (Fig. S2, Supporting information). Similar to other PAA/PVA nanofibers before and after immobilization of ZVI NPs or Fe/Pd bimetallic NPs, the Pd NP-immobilized fibrous mat displayed a smooth and uniform morphology with a mean diameter of 277 nm. ICP-AES elemental analysis of the aqua regia extract of the Pd NP-containing nanofibrous mats revealed that the Pd loading percentage within the nanofibers was 9.39%. Upon exposure of the colloid Fe/Pd NPs and the ZVI NP- and Fe/Pd NP-containing hybrid nanofibrous mats into an aqueous solution of TCE (10 mg/L), all the three systems were able to degrade TCE. The remaining fraction of TCE treated with Fe/Pd colloid NPs, ZVI NP- and Fe/Pd NP-immobilized nanofibrous mats was measured to be 0.41%, 0.88%, and 0.38%, respectively after 3.5 h. In contrast, the remaining fraction of TCE treated with Pd NP-immobilized nanofibrous mats was measured to be 93.04% under similar conditions, indicating that the immobilized Pd NPs within the PAA/PVA nanofibrous mats do not contribute to the dechlorination effect of TCE, and the slightly changed remaining fraction of TCE from 100% to 93.04% should be ascribed to the adsorption of TCE onto the polymer nanofibers with high specific surface area. The dechloridation reaction reached equilibrium for approximately 1.5 h. The more or less equivalent TCE removal efficiency using the above three different systems indicates that the NPs in either colloidal formulation or within nanofibrous mats are able to degrade the TCE. Although the Fe/Pd NP-immobilized nanofibrous mats are easy to be separated for further use, the initial low concentration of TCE (10 mg/L) does not allow the demonstration of the excellent performance of the Fe/Pd NP-immobilized nanofibrous mats in degradation of TCE.

In order to further investigate the enhanced dechlorination of TCE using Fe/Pd NP-immobilized nanofibrous mats, the initial TCE concentrations were increased to 20, 50, and 100 mg/L. An aliquot of the aqueous sample (10 mL) was withdrawn from the reactor after 1.5 h to analyze the residue TCE concentration. The TCE dechlorination efficiency was calculated according to Eq. (3). When the initial TCE concentration was increased to 20, 50, and 100 mg/L, the TCE dechlorination efficiency using Fe/Pd NP-containing nanofibrous mats remained above 90.6% for all cases, much higher than that using ZVI NP-containing nanofibrous mats and the Fe/Pd colloid NPs (Fig. 6). At a high initial TCE concentration (100 mg/L), the dechlorination efficiency of Fe/Pd NP-immobilized fibrous mats was as high as 95.9%. In contrast, the dechlorination efficiency of ZVI NP-immobilized mats and the colloidal Fe/Pd NPs was only 77.3% and 38.2%, respectively. The higher dechlorination efficiency of Fe/Pd NP-containing nanofibrous than that of Fe/Pd colloid NPs is presumably due to the much smaller size of the Fe/Pd NPs ($2.8 \pm 0.92$ nm) uniformly distributed in the polymer nanofibers with larger specific surface area, which favors the reactive degradation of TCE. In contrast, the colloid Fe/Pd NPs synthesized using the literature method display a wider size distribution (1–100 nm) and are prone to aggregation during the remediation process [35], resulting in lower dechlorination efficiency. The higher dechlorination efficiency of Fe/Pd NP-immobilized fibrous mats than ZVI NP-immobilized counterpart should be attributable to the catalytic effect of the metallic Pd deposited onto the ZVI NPs as mentioned in the Introduction. Detailed molecular mechanism regarding the dechlorination of TCE using Fe/Pd NPs has also been elaborated by He et al. [21] and Wang et al. [22].

The ionic strength and pH of the TCE aqueous solution may influence the TCE dechlorination efficiency of the Fe/Pd NP-immobilization nanofibrous mats. Therefore, we performed additional experiments related to the impact of pH and ionic strength (NaCl concentration) on the remediation efficiency of the Fe/Pd NP-immobilized fibrous mat. We show that under different ionic strengths ([NaCl] = 0 M, 0.1 M, 0.3 M, 0.5 M, 0.8 M, and 1 M), the TCE dechlorination efficiency of the hybrid nanofibers does not significantly change (Fig. S3, Supporting information). In addition, the effect of the pH of the TCE solution on the remediation efficiency of the Fe/Pd NP-immobilized fibrous mat was also investigated (Fig. S4, Supporting information). We show that in the pH range of 2.5–6.5, the TCE dechlorination activity of the bimetal-immobilized nanofibrous mat does not significantly change. Slightly higher dechlorination efficiency was observed under more acidic pH

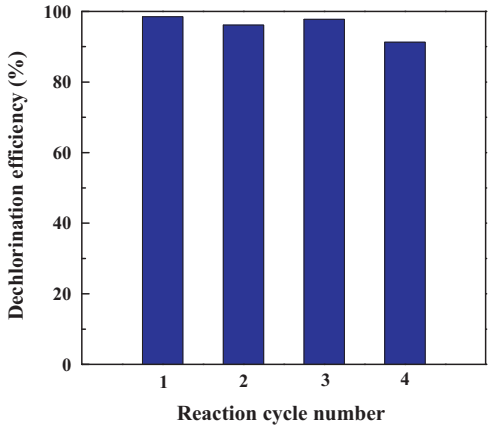


**Fig. 7.** Removal efficiency of TCE after treatment with the same Fe/Pd NP-containing nanofibrous mats for the first, second, third, and fourth time. The reaction time was 1.5 h and the initial TCE concentration was 10 mg/L.

conditions, which could be due to the less possibility to form metal oxide under acidic conditions during the remediation process.

For practical environmental applications, the reusability and recyclability of the NPs is of paramount importance. The Fe/Pd NP-containing nanofibrous mats developed in our study are reusable and recyclable. After exposure to sodium borohydride aqueous solution (0.94 M) for 10 min, the nanofibrous mats could be regenerated for further remediation process. The regenerated Fe/Pd NP-containing nanofibrous mats exhibited similar performance in the second, third, and fourth dechlorination experiments to that of the freshly prepared mats (Fig. 7). Similarly, the practical environmental remediation application of the NPs often requires the NPs to be easily recyclable after the remediation process, instead of leaving the particles dispersed in water to generate secondary contamination. When colloidal Fe/Pd NPs are used to degrade TCE, it is difficult to recycle the dispersed particles in wastewater. In sharp contrast, when Fe/Pd NPs immobilized within polymer nanofibers were exposed to water, it is easy to recycle the mats for further use. Furthermore, the Fe/Pd NPs immobilized within the fibrous mats are pretty stable, and do not leak from the mats during the remediation process. ICP-AES studies show that neither Fe nor Pd is released even if the Fe/Pd NP-immobilized fibrous mats are exposed to water for a month. This further demonstrates that the developed Fe/Pd NP-containing fibrous mats are very useful for practical environmental applications.

## 4. Conclusion

In summary, a facile approach to using electrospun polymer nanofibrous mats as a nanoreactor to immobilize bimetallic Fe/Pd NPs has been developed for environmental applications. The formed bimetallic Fe/Pd NPs with a mean diameter of 2.8 nm are uniformly distributed within the polymer nanofibers with a loading percentage of 21.88%. TCE dechlorination experiments reveal that the Fe/Pd bimetallic NPs immobilized within the polymer nanofibers are much more effective in remediation of TCE especially with high initial concentrations than the conventionally prepared colloid Fe/Pd NPs and the ZVI NPs immobilized within the same polymer nanofibers without further Pd deposition. With the high efficacy to stabilize the immobilized NPs, easiness to recycle and regenerate the NP-immobilized fibrous mats, as well as the high surface area to volume ratio and high porosity of the composite fibrous mats, the approach to immobilizing Fe/Pd bimetallic NPs within polymer nanofibers should be versatile and extendable to prepare various reactive NP systems for a range of environmental remediation applications.

## Acknowledgements

This research is financially supported by the Fundamental Research Funds for the Central Universities (for M.S., R.G., X.C., and X.S.), the Key Laboratory of Textile Science & Technology, Ministry of Education, "111 Project", B07024, and the Program for Professor of Special Appointment (Eastern Scholar) at Shanghai Institutions of Higher Learning. X.S. gratefully acknowledges the Fundação para a Ciência e a Tecnologia (FCT) and Santander bank for the Chair in Nanotechnology.

## Appendix A. Supplementary data

Supplementary data associated with this article can be found, in the online version, at doi:10.1016/j.jhazmat.2011.11.038.

## References

[1] W.S. Orth, R.W. Gillham, Dechlorination of trichloroethene in aqueous solution using $Fe^0$, Environ. Sci. Technol. 30 (1996) 66–71.
[2] Y.T. He, J.T. Wilson, R.T. Wilkin, Impact of iron sulfide transformation on trichloroethylene degradation, Geochim. Cosmochim. Acta 74 (2010) 2025–2039.
[3] R.J. Barnes, O. Riba, M.N. Gardner, T.B. Scott, S.A. Jackman, I.P. Thompson, Optimization of nano-scale nickel/iron particles for the reduction of high concentration chlorinated aliphatic hydrocarbon solutions, Chemosphere 79 (2010) 448–454.
[4] W. Lee, B. Batchelor, Abiotic reductive dechlorination of chlorinated ethylenes by iron-bearing soil minerals. 1. Pyrite and magnetite, Environ. Sci. Technol. 36 (2002) 5147–5154.
[5] M. Elsner, S.B. Haderlein, T. Kellerhals, S. Luzi, L. Zwank, W. Angst, R.P. Schwarzenbach, Mechanisms and products of surface-mediated reductive dehalogenation of carbon tetrachloride by Fe (II) on goethite, Environ. Sci. Technol. 38 (2004) 2058–2066.
[6] H.H. Cho, T. Lee, S.J. Hwang, J.W. Park, Iron and organo-bentonite for the reduction and sorption of trichloroethylene, Chemosphere 58 (2005) 103–108.
[7] Y. Liu, S.A. Majetich, R.D. Tilton, D.S. Sholl, G.V. Lowry, TCE dechlorination rates, pathways, and efficiency of nanoscale iron particles with different properties, Environ. Sci. Technol. 39 (2005) 1338–1345.
[8] W. Wang, M. Zhou, Z. Jin, T. Li, Reactivity characteristics of poly (methyl methacrylate) coated nanoscale iron particles for trichloroethylene remediation, J. Hazard. Mater. 173 (2010) 724–730.
[9] H. Kim, H.J. Hong, J. Jung, S.H. Kim, J.W. Yang, Degradation of trichloroethylene (TCE) by nanoscale zero-valent iron (nZVI) immobilized in alginate bead, J. Hazard. Mater. 176 (2010) 1038–1043.
[10] Y. Liu, T. Phenrat, G.V. Lowry, Effect of TCE concentration and dissolved groundwater solutes on NZVI-promoted TCE dechlorination and $H_2$ evolution, Environ. Sci. Technol. 41 (2007) 7881–7887.
[11] Q. Huang, X. Shi, R.A. Pinto, E.J. Petersen, W.J. Weber Jr., Tunable synthesis and immobilization of zero-valent iron nanoparticles for environmental applications, Environ. Sci. Technol. 42 (2008) 8884–8889.
[12] X. Wang, C. Chen, H. Liu, J. Ma, Preparation and characterization of PAA/PVDF membrane-immobilized Pd/Fe nanoparticles for dechlorination of trichloroacetic acid, Water Res. 42 (2008) 4656–4664.
[13] F. He, D. Zhao, Preparation and characterization of a new class of starch-stabilized bimetallic nanoparticles for degradation of chlorinated hydrocarbons in water, Environ. Sci. Technol. 39 (2005) 3314–3320.
[14] B. Schrick, J.L. Blough, A.D. Jones, T.E. Mallouk, Hydrodechlorination of trichloroethylene to hydrocarbons using bimetallic nickel–iron nanoparticles, Chem. Mater. 14 (2002) 5140–5147.
[15] Y.H. Tee, E. Grulke, D. Bhattacharyya, Role of Ni/Fe nanoparticle composition on the degradation of trichloroethylene from water, Ind. Eng. Chem. Res. 44 (2005) 7062–7070.
[16] W. Zhang, C.B. Wang, H.L. Lien, Treatment of chlorinated organic contaminants with nanoscale bimetallic particles, Catal. Today 40 (1998) 387–395.
[17] N.E. Korte, J.L. Zutman, R.M. Schlosser, L. Liang, B. Gu, Q. Fernando, Field application of palladized iron for the dechlorination of trichloroethene, Waste Manag. 20 (2000) 687–694.
[18] I.F. Cheng, Q. Fernando, N. Korte, Electrochemical dechlorination of 4-chlorophenol to phenol, Environ. Sci. Technol. 31 (1997) 1074–1078.
[19] W. Zhang, Nanoscale iron particles for environmental remediation: an overview, J. Nanopart. Res. 5 (2003) 323–332.
[20] H. Choi, S.R. Al-Abed, S. Agarwal, Effects of aging and oxidation of palladized iron embedded in activated carbon on the dechlorination of 2-chlorobiphenyl, Environ. Sci. Technol. 43 (2009) 4137–4142.

[21] F. He, D. Zhao, Hydrodechlorination of trichloroethene using stabilized Fe–Pd nanoparticles: reaction mechanism and effects of stabilizers, catalysts and reaction conditions, Appl. Catal. B 84 (2008) 533–540.
[22] X. Wang, C. Chen, H. Liu, J. Ma, Characterization and evaluation of catalytic dechlorination activity of Pd/Fe bimetallic nanoparticles, Ind. Eng. Chem. Res 47 (2008) 8645–8651.
[23] F. He, D. Zhao, J. Liu, C.B. Roberts, Stabilization of Fe–Pd nanoparticles with sodium carboxymethyl cellulose for enhanced transport and dechlorination of trichloroethylene in soil and groundwater, Ind. Eng. Chem. Res 46 (2007) 29–34.
[24] Y.H. Lin, H.H. Tseng, M.Y. Wey, M.D. Lin, Characteristics, morphology, and stabilization mechanism of PAA250K-stabilized bimetal nanoparticles, Colloids Surf. A: Physicochem. Eng. Aspects 349 (2009) 137–144.
[25] H. Choi, S.R. Al-Abed, Effect of reaction environments on the reactivity of PCB (2-chlorobiphenyl) over activated carbon impregnated with palladized iron, J. Hazard. Mater. 179 (2010) 869–874.
[26] H. Choi, S.R. Al-Abed, S. Agarwal, D.D. Dionysiou, Synthesis of reactive nano-Fe/Pd bimetallic system-impregnated activated carbon for the simultaneous adsorption and dechlorination of PCBs, Chem. Mater. 20 (2008) 3649–3655.
[27] J. Xu, D. Bhattacharyya, Modeling of Fe/Pd nanoparticle-based functionalized membrane reactor for PCB dechlorination at room temperature, J. Phys. Chem. C 112 (2008) 9133–9144.
[28] K. Venkatachalam, X. Arzuaga, N. Chopra, V.G. Gavalas, J. Xu, D. Bhattacharyya, B. Hennig, L.G. Bachas, Reductive dechlorination of 3,3′,4,4′-tetrachlorobiphenyl (PCB77) using palladium or palladium/iron nanoparticles and assessment of the reduction in toxic potency in vascular endothelial cells, J. Hazard. Mater. 159 (2008) 483–491.
[29] J. Xu, D. Bhattacharyya, Fe/Pd nanoparticle immobilization in microfiltration membrane pores: synthesis, characterization, and application in the dechlorination of polychlorinated biphenyls, Ind. Eng. Chem. Res. 46 (2007) 2348–2359.
[30] S. Xiao, H. Ma, M. Shen, S. Wang, Q. Huang, X. Shi, Excellent copper(II) removal using zero-valent iron nanoparticle-immobilized hybrid electrospun polymer nanofibrous mats, Colloids Surf. A: Physicochem. Eng. Aspects (2011), doi:10.1016/j.colsurfa.2011.1003.1005.
[31] S. Xiao, S. Wu, M. Shen, R. Guo, Q. Huang, S. Wang, X. Shi, Polyelectrolyte multilayer-assisted immobilization of zero-valent iron nanoparticles onto polymer nanofibers for potential environmental applications, ACS Appl. Mater. Interfaces 1 (2009) 2845–2855.
[32] S.L. Xiao, M.W. Shen, R. Guo, Q.G. Huang, S.Y. Wang, X.Y. Shi, Fabrication of multiwalled carbon nanotube-reinforced electrospun polymer nanofibers containing zero-valent iron nanoparticles for environmental applications, J. Mater. Chem. 20 (2010) 5700–5708.
[33] S.L. Xiao, M.W. Shen, R. Guo, S.Y. Wang, X.Y. Shi, Immobilization of zerovalent iron nanoparticles into electrospun polymer nanofibers: synthesis, characterization, and potential environmental applications, J. Phys. Chem. C 113 (2009) 18062–18068.
[34] X. Fang, H. Ma, S. Xiao, M. Shen, R. Guo, X. Cao, X. Shi, Facile immobilization of gold nanoparticles into electrospun polyethyleneimine/polyvinyl alcohol nanofibers for catalytic applications, J. Mater. Chem. 21 (2011).
[35] B.W. Zhu, T.T. Lim, Catalytic reduction of chlorobenzenes with Pd/Fe nanoparticles: reactive sites catalyst stability, particle aging, and regeneration, Environ. Sci. Technol. 41 (2007) 7523–7529.
[36] X. Wang, C. Chen, Y. Chang, H. Liu, Dechlorination of chlorinated methanes by Pd/Fe bimetallic nanoparticles, J. Hazard. Mater. 161 (2009) 815–823.
[37] M.V. Nesterova, S.A. Walton, J. Webb, Nanoscale iron (III) oxyhydroxy aggregates formed in the presence of functional water-soluble polymers: models for iron (III) biomineralisation processes, J. Inorg. Biochem. 79 (2000) 109–118.